Cell Reports, Volume *36*

Supplemental information

The neutralization potency of anti-SARS-CoV-2 therapeutic human monoclonal antibodies is retained against viral variants

Efi Makdasi, Anat Zvi, Ron Alcalay, Tal Noy-Porat, Eldar Peretz, Adva Mechaly, Yinon Levy, Eyal Epstein, Theodor Chitlaru, Ariel Tennenhouse, Moshe Aftalion, David Gur, Nir Paran, Hadas Tamir, Oren Zimhony, Shay Weiss, Michal Mandelboim, Ella Mendelson, Neta Zuckerman, Ital Nemet, Limor Kliker, Shmuel Yitzhaki, Shmuel C. Shapira, Tomer Israely, Sarel J. Fleishman, Ohad Mazor, and Ronit Rosenfeld

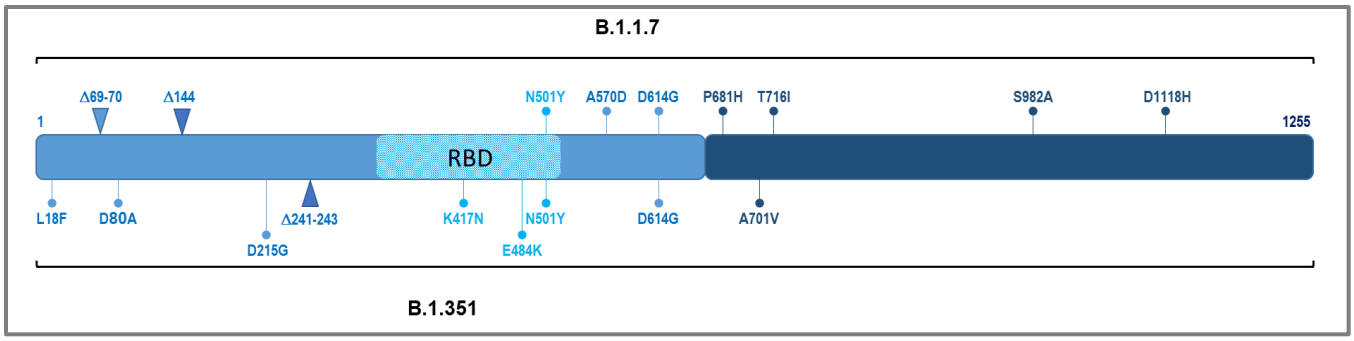

Figure S1. Schematic representation of SARS-CoV-2 spike variants. Related to Figures 1, 3 and 4. Schematic depiction of the SARS-CoV-2 spike, along with the replacements and deletions characterizing the SARS-CoV-2 B.1.1.7 and B.1.351 genetic variants. The numbering is according to the Wuhan reference sequence (Accession no. NC_045512).

We previously reported the classification of human antibodies targeting the SARS-CoV-2 RBD at four distinct epitopes, represented by MD65, MD62, MD29 and MD47 mAbs (Noy-Porat et al., 2020). At the current study, BL6 mAb, targeting a competing epitope with the MD47 (Noy-Porat et al., 2020), was included. In the figure below, binning analysis of the BL6 with each of the other mAbs studied herein, is presented (panel A). Additionally, for the completion of studied mAbs characteristics (summarized at Supplementary table 1), the hACE2 binding inhibition by BL6, is also presented (panel B).

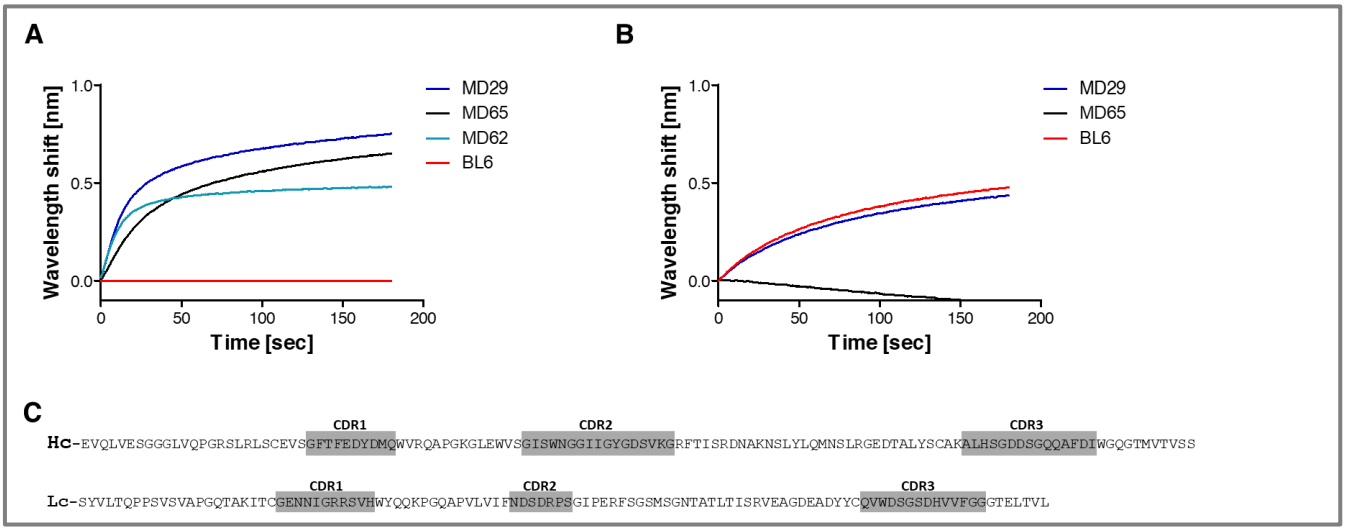

Figure S2. Epitope binning and ACE2 competition of BL6 determined by BLI analysis. Related to STAR Methods. **A**. Streptavidin-coated biosensors were loaded with biotinylated BL6 antibody and incubated for 300 seconds with the monomeric RBD, washed and then incubated with the indicated antibodies for another 300 seconds. Only the last step of the analysis is presented. Background signal was obtained from a parallel sensor incubated with the homologous antibody and sensograms are presented after subtraction of the background signal. **B**. Binding of human ACE2 to RBD in the presence of BL6, MD29 (negative control) and MD65 (positive control) was tested by BLI. Each of the antibodies was immobilized on a protein A sensor, saturated with RBD, washed and incubated with recombinant human ACE2 for 300 s. Time 0 represents the binding of the ACE2 to the antibody- RBD complex. **C**. The full-length amino acid sequence of the heavy (Hc) and light chain (Lc) variable domains for BL6. CDRs domains are colored in gray.

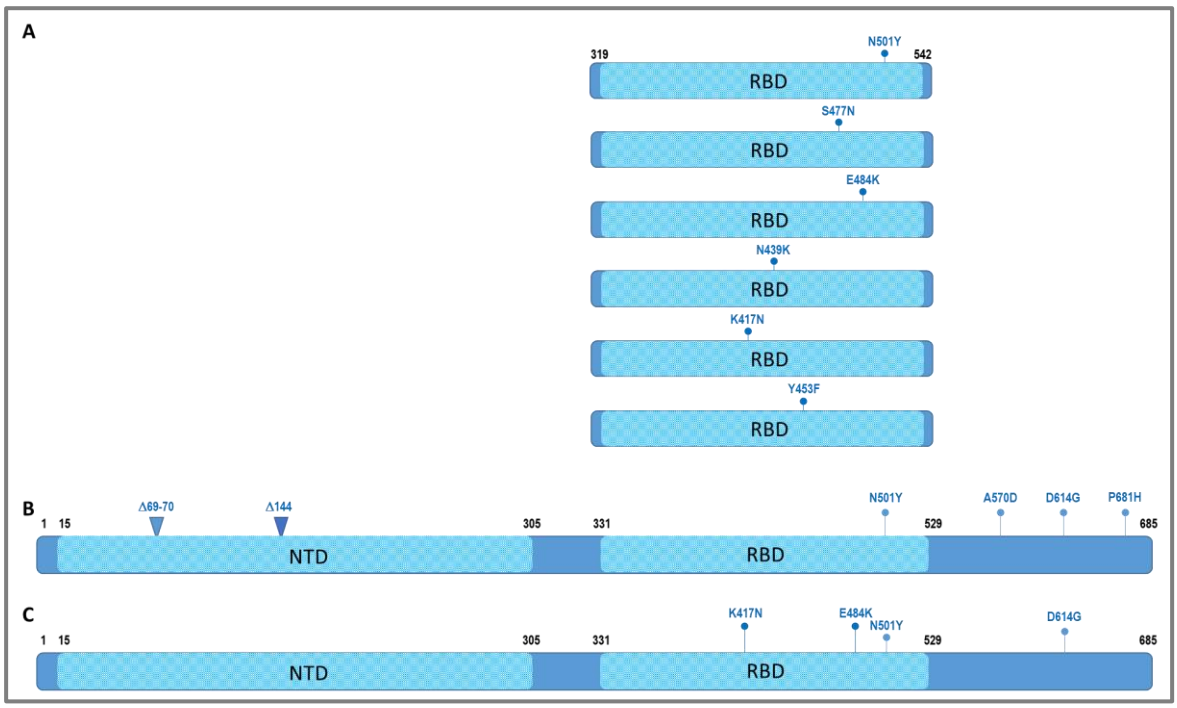

Figure S3. Schematic representation of SARS-CoV-2 RBD and S1 variants. Related to Figure 1 and 3. **A**. Depiction of recombinant RBD variant proteins, each including the indicated single highly frequent replacements reported in the RBD domain. The domain coordinates are according to the recombinant RBD used throughout the study. **B**. Schematic representation of the spike S1 subunit, along with the replacements and deletions characterizing the SARS-CoV-2 B.1.1.7 genetic variant. **C**. Schematic representation of the spike S1 subunit, along with the RBD replacements, characterizing the SARS-CoV-2 B.1.351 genetic variant. The numbering is according to the Wuhan reference sequence (Accession no. NC_045512). For the full panel of replacements in the B.1.1.7 and B.1.351 spike protein, see Supplementary Figure 1.

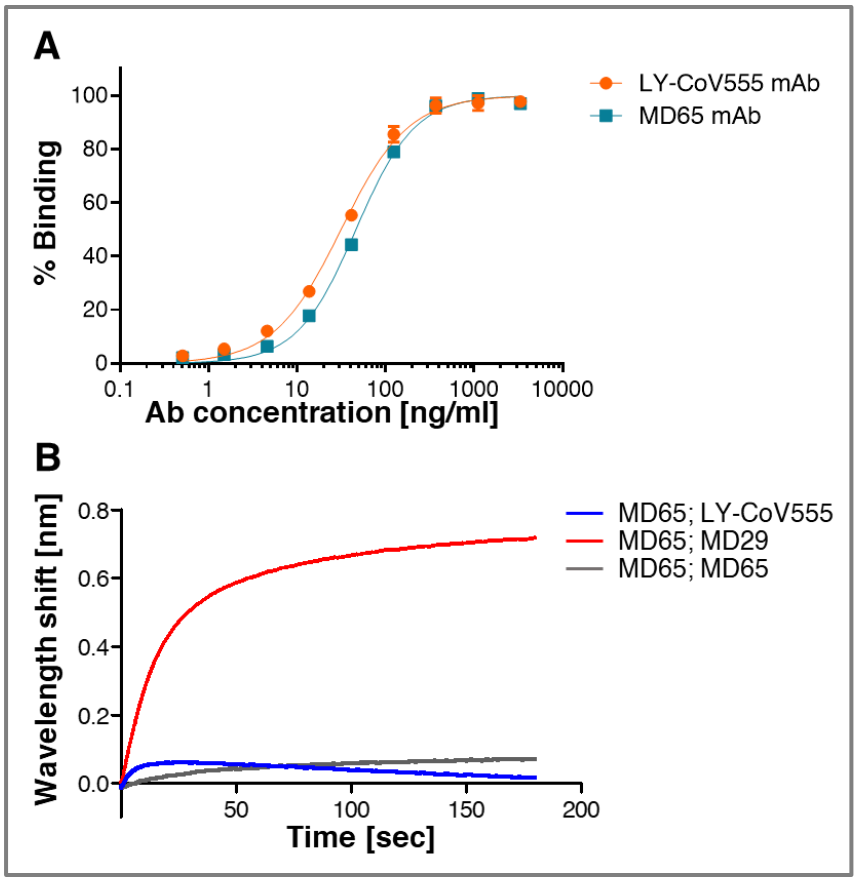

Figure S4. Binding characterization of the LY-CoV555 mAb (Bamlanivimab). Related to Figure 1 and 3. **A.** Binding of the LY-CoV555 and MD65 mAbs was evaluated by ELISA against SARS-CoV-2 spike protein, demonstrating similar binding profiles. Data shown represent average of triplicates ±SEM. **B.** BLI was applied for epitope binning experiments. MD65 antibody was biotinylated, immobilized on a streptavidin sensor and saturated with WT rRBD protein. The complex was then incubated for 180 s with LY-CoV555 or MD29 and MD65 as controls. Time 0 represents the binding to the MD65-rRBD complex. LY-CoV555 failed to bind the rRBD protein, presented in complex with MD65 mAb, while significant binding was observed when the rRBD was presented in complex with MD29 (which binds a different epitope than MD65). These results clearly indicate that LY-CoV555 and MD65 target overlapping epitopes.

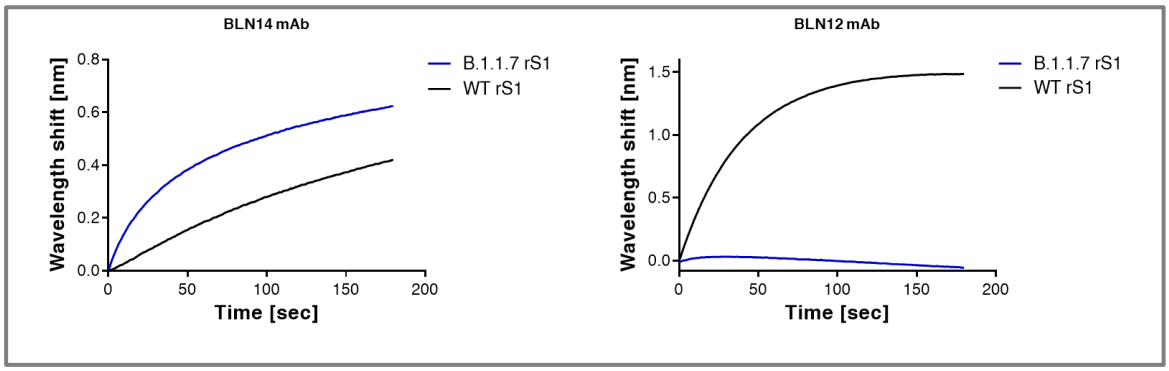

Figure S5. Binding of rS1 variants by NTD-specific mAbs. Related to Figure 4. Biolayer interferometry (BLI) was applied for evaluating the ability of BLN14 and BLN12 mAbs, directed to the SARS-CoV-2 spike NTD, to bind the recombinant multiple-mutated spike S1 subunit protein: B.1.1.7 rS1 [Δ 69-70; Δ 144; N501Y; A570D; D614G; P681H]. Each of the mAbs, was immobilized on a protein-A sensor and incubated for 180 sec with B.1.1.7 (blue) or with the WT rS1 (black). The figure includes representative graphs of two independent experimental repeats, yielding similar results.

Table S1. Properties of anti-RBD and anti-NTD neutralizing mAbs.

mAb	Subdomain specificity	K_D (nM)	ACE2 binding inhibition	S1 Binding[d]			PRNT IC_{50} (µg/ml)		
				w.t	B.1.1.7	B.1.351	w.t	B.1.1.7	B.1.351
MD29	RBD	0.4[a]	No [a]	1.0	0.92	0.88	7.8	3.0	12.9
MD62	RBD	4.8 [a]	yes [a]	1.0	0.5	0.06	1.9	2.0	>10000
MD65	RBD	2.5 [a]	yes [a]	1.0	1.38	0.34	0.1	0.04	0.4
BL6	RBD	1.1[b]	No	1.0	1.0	0.79	0.7	0.08	2.3
BLN12	NTD	0.9 [c]	No [c]	1.0	0.02	N.A	0.07	4.8	98.0
BLN14	NTD	12.7 [c]	No [c]	1.0	1.86	N.A	0.07	0.04	>10000

[a] (Noy-Porat et al., 2020); [b] (Barlev-Gross et al., 2021); [c] (Noy-Porat et al., 2021); [d] relative binding compared to w.t according to AUC calculation; N.A- not assessed ; IC_{50} >10,000 indicates complete loss of neutralization capacity. Related to Figures 3 and 4.